

Slip Flow of a Shear-Thinning Power-Law Fluid Past an Assemblage of Spherical Particles

Rahul R. Ramteke and Nanda Kishore

Abstract The momentum transfer characteristics of slip flow around an assemblage of spherical particles in a shear-thinning fluid ($n = 0.6$) is numerically studied. At fluid-solid interface a linear slip velocity is applied. As the non-dimensional slip number (λ) increases, the fluid slip becomes weaker i.e., $\lambda = 0$ represents fully slip flow and $\lambda = \infty$ indicate no-slip velocity at the solid-fluid interface. A finite difference method based on SMAC semi-implicit algorithm is used in this work over the range of conditions as: Reynolds number, $Re = 100$ – 200 , power-law behavior index, $n = 0.6$, volume fraction of slip spheres, $\Phi = 0.1$, and dimensionless slip parameter, $\lambda = 0.01$ – 100 . Finally effects of these parameters on detailed flow kinematics are discussed in details.

Keywords Slip flow • Spheres • Cell model • Reynolds number • Shear thinning fluid • Drag coefficient • Slip number

Nomenclature

C_d	Total drag coefficient
C_{df}	Friction drag coefficient
C_{dp}	Pressure drag coefficient
F_d	Drag force (N)
p	Pressure
r	Radial distance
R	Sphere radius (m)
λ	Slip number
Re	Reynolds number
R_∞	Cell boundary

R.R. Ramteke · Nanda Kishore (✉)

Department of Chemical Engineering, Indian Institute of Technology Guwahati,
Guwahati 781039, Assam, India

e-mail: nkishore@iitg.ernet.in

© Springer India 2017

A.K. Saha et al. (eds.), *Fluid Mechanics and Fluid*

Power – Contemporary Research, Lecture Notes in Mechanical Engineering,

DOI 10.1007/978-81-322-2743-4_2

U	Free stream velocity (m/s)
v_r	r-component of velocity
v_θ	θ -component of velocity

Greek Symbols

Φ	Volume fraction of slip spheres
ε	Rate of strain tensor
η	Fluid viscosity
ρ	Fluid density (kg/m^3)
τ	Extra stress tensor

1 Introduction

The solution of fluid flow past solid particles with no-slip boundary condition at the fluid-solid interface is mostly used assumption in fluid mechanics. But the no-slip condition is not valid in case of flow in micro/nano-channels, aerosol particles, flow through porous media and variety of complex fluids such as polymer solution, molten polymer, emulsion and foam [1–4]. Because of violation of no-slip boundary condition, researchers have chosen the slip boundary condition due to its range of applications in micro and nano-fluidic devices. However, fluid-slip at the solid surface can occur even at macroscopic level especially in the case of polymer extrusion, flow of non-Newtonian fluids through pipes/channels, etc. Further adequate experimental evidence is available on Newtonian and non-Newtonian fluids slip along the solid boundaries [6–10]. Excellent reviews are available which discussed Newtonian [11] and non-Newtonian fluid slip flow over solid surface [1, 5]. The fluid flow past single spherical particle with slip boundary condition at the fluid-solid sphere interface has been studied analytically and numerically by several researchers [12–17]. But occurrence of fluid flow over assemblages of particle such as oil through porous material, catalytic cracking process in oil industries, filtration of polymer solution and slurries, fluidization etc. is very common in many processing industries. Because of wide range of applications, studies on flow past assemblages of particles gain more attention using cell model. In particular, cell model is mostly used to investigate the effect of volume fraction of particles on overall fluid flow past assemblages of particles. In the cell model, an assemblage can be uniformly divided into number of identical hypothetical envelopes of continuous fluid and every particle is surrounded by the hypothetical envelope of continuous fluid. Thus a multiparticle system reduces to single particle system yet counting for effect of volume fraction on the overall drag and heat/mass transfer characteristics. Faltas and Saad [18] studied Stokes flow ($Re \rightarrow 0$) past assemblages of slip spherical particles using free surface cell model [19] and zero vorticity cell

model [20] with a linear slip boundary condition at the interface. In this work, a shear-thinning power-law fluid ($n = 0.6$) flow past an assemblage of slip spheres (of volume fraction $\Phi = 0.1$) is numerically investigated using a combination of a linear slip model and Happel's free surface cell model in the range of $Re = 100$ – 200 and slip number $\lambda = 0.01$ – 100 .

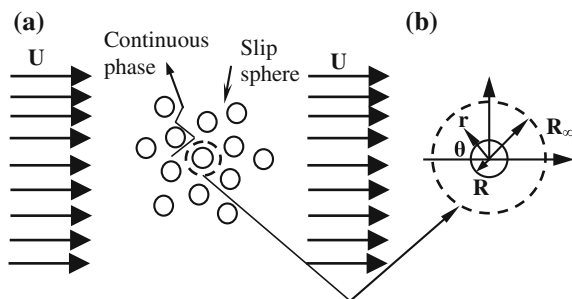
2 Problem Statement

Flow of an incompressible shear thinning fluid through an assemblage of slip spherical particles is considered as shown in Fig. 1. The flow is assumed to be steady and axisymmetric; and the degree of slip at the solid—fluid interface for all particles is constant. The effect of volume fraction of slip spheres on overall momentum transfer characteristics are considered within the framework of free surface cell model due to Happel [19]. To account the fluid-slip, a linear slip boundary condition is applied at fluid-solid interface in which the slip velocity at the solid surface is proportional to the shear stress. The governing conservation equations of mass and momentum along with boundary conditions are converted to non-dimensional form using the following scaling parameters. The radial distance is scaled by radius of sphere “ R ”, velocity components are scaled using free stream velocity U , pressure terms are scaled using $\{\rho U^2\}$, shear stress is normalized using $\{m(U/R)^n\}$ and the non-Newtonian fluid viscosity is normalized by a reference (or apparent) viscosity (η_{ref}). The final dimensionless governing continuity and momentum equations can be written as follows:

- Continuity equation

$$\frac{1}{r^2} \frac{\partial}{\partial r} [r^2 v_r] + \frac{1}{r \sin \theta} \frac{\partial}{\partial \theta} [v_\theta \sin \theta] = 0 \quad (1)$$

Fig. 1 Schematic representation of flow past an assemblage of spherical particles



- r —component of momentum equation

$$\begin{aligned} \frac{\partial v_r}{\partial t} + \frac{1}{r^2} \frac{\partial}{\partial r} [r^2 v_r^2] + \frac{1}{r \sin \theta} \frac{\partial}{\partial \theta} [v_r v_\theta \sin \theta] - \frac{v_\theta^2}{r} = & -\frac{\partial p}{\partial r} + \frac{2^{n+1}}{\text{Re}} \left[\varepsilon_{rr} \frac{\partial \eta}{\partial r} + \frac{\varepsilon_{r\theta}}{r} \frac{\partial \eta}{\partial \theta} \right] \\ & + \frac{2^n \eta}{\text{Re}} \left[\frac{1}{r^2} \frac{\partial^2}{\partial r^2} (r^2 v_r) + \frac{1}{r^2 \sin \theta} \frac{\partial}{\partial \theta} \left(\sin \theta \frac{\partial v_r}{\partial \theta} \right) \right] \end{aligned} \quad (2)$$

- θ —component of momentum equation

$$\begin{aligned} \frac{\partial v_\theta}{\partial t} + \frac{1}{r^2} \frac{\partial}{\partial r} [r^2 v_r v_\theta] + \frac{1}{r \sin \theta} \frac{\partial}{\partial \theta} [v_\theta^2 \sin \theta] + \frac{v_r v_\theta}{r} = & -\frac{1}{r} \frac{\partial p}{\partial \theta} + \frac{2^{n+1}}{\text{Re}} \left[\varepsilon_{r\theta} \frac{\partial \eta}{\partial r} + \frac{\varepsilon_{\theta\theta}}{r} \frac{\partial \eta}{\partial \theta} \right] \\ & + \frac{2^n \eta}{\text{Re}} \left[\frac{1}{r^2} \frac{\partial}{\partial r} \left(r^2 \frac{\partial v_\theta}{\partial r} \right) + \frac{1}{r^2} \frac{\partial}{\partial \theta} \left(\frac{1}{\sin \theta} \frac{\partial}{\partial \theta} [v_\theta \sin \theta] \right) + \frac{2}{r^2} \frac{\partial v_r}{\partial \theta} \right] \end{aligned} \quad (3)$$

The Reynolds number for power-law liquids is defined as follows:

$$\text{Re} = \frac{\rho U^{(2-n)} (2R)^n}{m} \quad (4)$$

For an incompressible liquid, components of extra stress tensor are related to the rate of deformation tensor as follows:

$$\tau_{ij} = 2\eta \varepsilon_{ij}; \quad \text{where } i, j = r, \theta, \phi \quad (5)$$

The power-law fluid viscosity is given by:

$$\eta = \left(\frac{\Pi_\varepsilon}{2} \right)^{(n-1)/2} \quad (6)$$

where Π_ε is the second invariant of rate of deformation tensor which can be expressed in terms of derivatives of velocity components [21].

The following dimensionless boundary conditions are found to be appropriate for this slip flow problem:

- Along the surface of slip sphere ($r = 1, \theta = 0, \pi$)

$$v_r = 0; \tau_{r\theta} = \lambda \times v_\theta \quad (7a)$$

- At the outer cell boundary ($r = R_\infty, \theta = 0, \pi$)

$$v_r = -\cos \theta; \tau_{r\theta} = 0 \quad (7b)$$

- Along the axis of symmetry ($\theta = 0, \pi$)

$$v_\theta = 0; \frac{\partial v_r}{\partial \theta} = 0 \quad (7c)$$

The governing continuity and momentum equations subject to aforementioned boundary conditions are numerically solved to obtain the fully converged velocity and the pressure. From known velocity and pressure fields, the streamlines and vorticity distributions, surface pressure, vorticity distributions and drag coefficients can be evaluated. The total drag coefficient (C_d) is defined as:

$$C_d = \frac{2F_d}{\rho U^2 A_P} = C_{dp} + C_{df} \quad (8)$$

The pressure component (C_{dp}) is evaluated as:

$$C_{dp} = 2 \int_0^\pi [p \sin 2\theta]_{r=1} d\theta \quad (9)$$

and the frictional component (C_{df}) is evaluated as:

$$C_{df} = \frac{2^{n+2}}{\text{Re}} \int_0^\pi \left\{ \eta \left[\left(\frac{\partial v_\theta}{\partial r} - \frac{v_\theta}{r} \right) \sin^2 \theta - \left(\frac{\partial v_r}{\partial r} \right) \sin 2\theta \right] \right\}_{r=1} d\theta \quad (10)$$

The vorticity ($\omega_{r\theta}$) and stream functions (ψ) in spherical coordinates can be written as follows:

$$\omega_{r\theta} = \frac{\partial v_\theta}{\partial r} + \frac{v_\theta}{r} - \frac{1}{r} \frac{\partial v_r}{\partial \theta} \quad (11)$$

$$\frac{\partial^2 \psi}{\partial r^2} + \frac{\sin \theta}{r^2} \frac{\partial}{\partial \theta} \left(\frac{1}{\sin \theta} \frac{\partial \psi}{\partial \theta} \right) = \omega_{r\theta} r \sin \theta \quad (12)$$

3 Numerical Methodology

A finite difference method based semi-implicit simplified marker and cell (SMAC) method is used to solve governing equations of continuity and momentum, i.e. Eqs. (1)–(3) subjected to boundary conditions mentioned in Eq. (7a)–(7c). This scheme is implemented on a staggered grid arrangement in spherical coordinates. This algorithm is a simplified version of marker and cell (MAC) method introduced by Harlow and Welch [22]. The diffusive and non-Newtonian terms of the

momentum equation are discretized using second order central difference scheme whereas convective terms are discretized using quadratic upstream interpolation for convective kinematics (QUICK) scheme by Leonard [23]. The false-transient time stepping method is used to obtain steady state solution, which is the reason for retaining transient terms in the momentum equations.

3.1 Grid Independence Study

Table 1 shows the effect of grid size (in r and θ directions) for the case of slip flow of a shear-thinning fluid of $n = 0.6$ over an assemblage of spherical particles of hold-up $\Phi = 0.1$ at $Re = 200$ for either extremes of slip number i.e., for $\lambda = 0.01$ and $\lambda = 100$. It can be seen from this table that grids 60×60 and 90×60 produce almost identical values; however the CPU time for convergence with the grid 90×60 is three folds larger as compared to that of grid 60×60 . Thus grid 60×60 has been chosen for all other computations.

3.2 Validation

For $n = 0.6$ and $Re = 1$, in the limits of $\lambda = 0.01$ and $\lambda = 1000$, the present predictions on drag coefficients of slip spheres are compared with existing literature results for swarms of bubbles and assemblages of no-slip spheres, respectively and presented in Table 2. It can be seen from this table that the agreement between two values is within $\pm 4-5$ %.

Table 1 Effect of grid on drag of assemblage of slip spheres ($\Phi = 0.1$) in shear-thinning fluids of $n = 0.6$ at $Re = 200$

Grid	$\lambda = 0.01$			$\lambda = 100$		
	C_{dp}	C_{df}	C_d	C_{dp}	C_{df}	C_d
30×30	0.1364	0.0746	0.2110	0.6421	0.2292	0.8713
60×30	0.1346	0.0745	0.2101	0.6548	0.2378	0.8926
60×60	0.1345	0.0760	0.2105	0.7431	0.2386	0.9817
90×60	0.1344	0.0762	0.2106	0.7465	0.2425	0.9890

Table 2 Comparison of present C_d values with previous literature values at $Re = 1$ and for $n = 0.6$ in either extremis of $\lambda = 0.01$ (fully slip bubbles) and $\lambda = 1000$ (no slip spheres)

Present	Fully slip bubbles [24]	Present	No-slip solid spheres [25]
$\Phi = 0.1$		$\Phi = 0.0001$	
21.611	21.264	29.865	30.9517

4 Results and Discussion

4.1 Flow Patterns

Figure 2 shows streamlines (upper half) and iso-vorticity (lower half) contours for the case of a shear-thinning fluid ($n = 0.6$) flow past an assemblage of holdup $\Phi = 0.1$ at $Re = 100$ (a–c) and 200 (d–f). For both values of the Reynolds number, streamlines are showing fore and aft symmetry for full slip condition ($\lambda = 0.01$). The motion of the fluid around sphere is smoother for both Reynolds numbers. The amount of vorticity created increases with increasing slip number and the vorticity carried along the flow direction. However, recirculation wake is observed at the rear end of slip sphere for $\lambda \geq 10$ and its size increases with increasing slip number. This is due to the decrease of the fluid slip at the solid surface with increasing slip number. Thus amount of vorticity that is created around the sphere is increased with the slip number. The angle of flow separation increased with increasing slip number for both values of Re .

4.2 Surface Vorticity

Figure 3 shows the effect of slip number on the vorticity distribution along the surface of slip spheres in an assemblage of slip spheres of holdup $\Phi = 0.1$ in a power-law shear thinning fluid of $n = 0.6$ at $Re = 100$ and 200. The surface vorticity is zero at the front stagnation point and increases while traversing from front

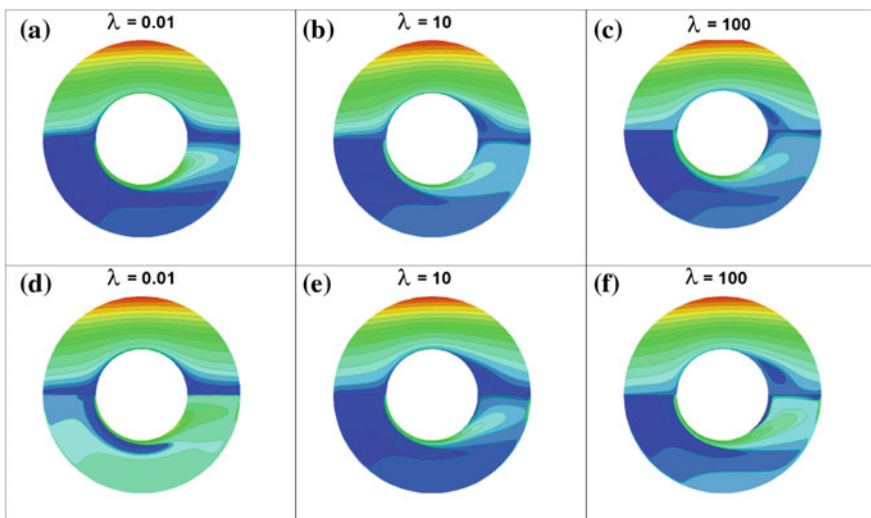


Fig. 2 Streamlines (*upper half*) and vorticity (*lower half*) contours in an assemblage of slip spheres of holdup $\Phi = 0.1$ in shear-thinning fluid ($n = 0.6$) at $Re = 100$ (a–c) and $Re = 200$ (d–f)

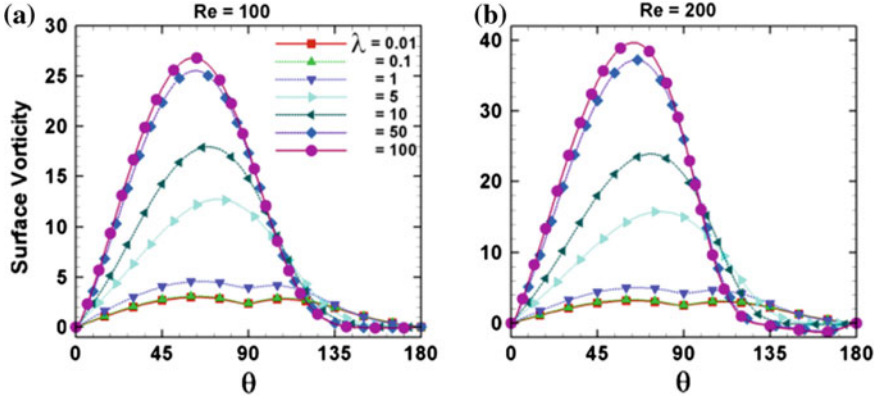


Fig. 3 Surface vorticity distribution on the surface of slip sphere in an assemblage of holdup $\Phi = 0.1$ in a shear thinning fluid of $n = 0.6$. **a** $Re = 100$. **b** $Re = 200$

stagnation point to around $\theta \sim 60^\circ$, and gradually decreases while traversing toward rear stagnant point. For two values of Reynolds number, in the rear end of sphere a secondary wake is observed for $\lambda \geq 10$ which is because of formation of recirculation wake. The surface vorticity magnitude increases with increasing slip number at around $\theta \sim 60^\circ$ and this magnitude increases with increasing Reynolds numbers. The surface vorticity is minimum for $\lambda = 0.01$ and maximum for $\lambda = 100$ around $\theta \sim 60^\circ$. For intermediate values of the slip number, surface vorticity magnitude lies between vorticity magnitude for $\lambda = 0.01$ and 100.

4.3 Surface Pressure Coefficient

Figure 4 shows the effect of slip numbers on pressure coefficient distribution along the surface of slip spheres in an assemblage of slip spheres of holdup $\Phi = 0.1$ in a power-law shear thinning fluid of $n = 0.6$ at $Re = 100$ and 200. For both values of Re , the surface pressure coefficient decreases while traversing from front stagnant point to around equator and it increases while traversing from around equator to rear stagnant point. This trend is similar for all slip numbers. The pressure recovery in rear half of spherical particle increases with decreasing slip number, i.e., the recovery of the pressure is large in the case of full slip $\lambda = 0.01$ and it is poor in the case of large slip number. As the slip number increases from $\lambda = 0.01$ to 100, the surface pressure coefficient increases at the front stagnant point and it decreases at around equator $\theta = 90^\circ$ for both $Re = 100$ and 200. The value of the surface pressure coefficient is minimum for slip number $\lambda = 0.01$ and maximum for $\lambda = 100$, whereas for intermediate slip numbers pressure coefficient lies between these two limiting values from the front stagnation point to equator; however, opposite trend observed from $\theta \approx 110-120^\circ$ to rear stagnation point.

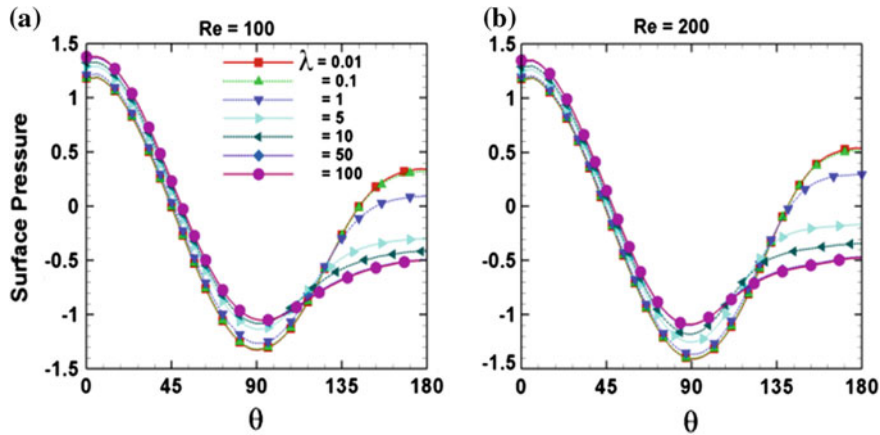


Fig. 4 Surface pressure coefficient on the surface of slip sphere in an assemblage of holdup $\Phi = 0.1$ in a shear thinning fluid of $n = 0.6$. **a** $Re = 100$. **b** $Re = 200$

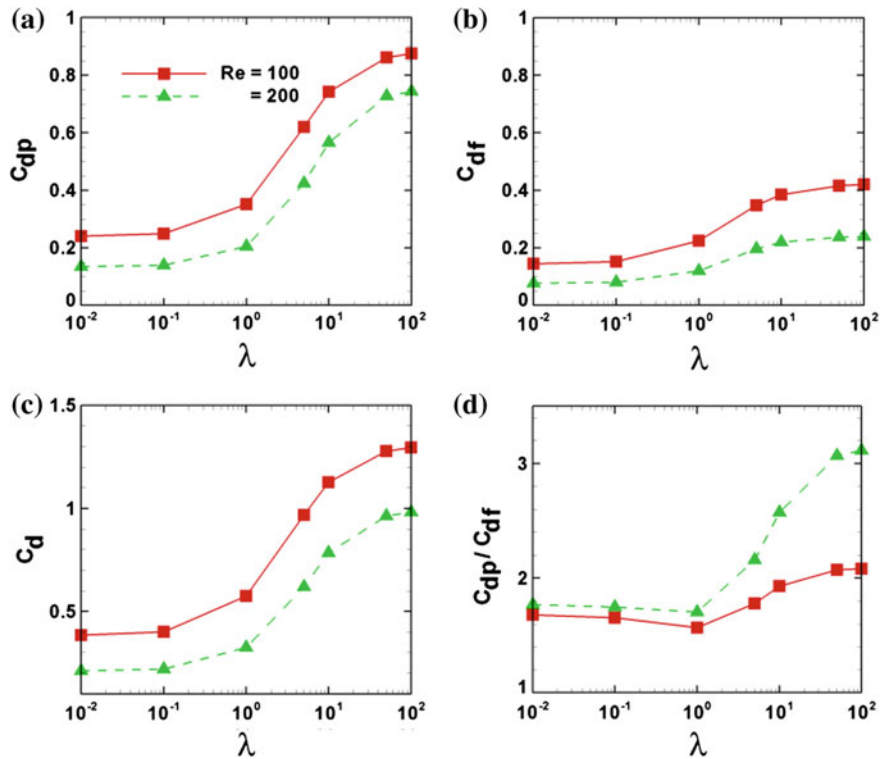


Fig. 5 Drag coefficients and drag ratio of an assemblage of slip sphere of holdup $\Phi = 0.1$ in a shear thinning fluid of $n = 0.6$

4.4 Drag Coefficient

Figure 5 shows the effect of different slip at Reynolds numbers $Re = 100$ and 200 on the drag coefficients and drag ratio (between pressure drag to friction drag) of assemblage of slip spheres of holdup $\Phi = 0.1$ in a shear thinning fluid of $n = 0.6$. The force exerted by fluid on the surface of spherical particles contains pressure drag and viscous drag. The total drag coefficient is the combination of pressure drag coefficient and friction drag coefficient. The total drag coefficients decreases and drag ratios increases with increasing Reynolds numbers from $Re = 100$ to 200 . The individual and total drag coefficients increase with increasing slip number up to $\lambda = 50$, after that they remain almost constant with increasing slip number for both $Re = 100$ and 200 . Therefore, it can be concluded that the individual and total drag coefficients of assemblages of slip spheres decreases with decreasing λ and/or with increasing Re .

5 Conclusion

Slip flow of a shear thinning fluid ($n = 0.6$) past an assemblage of $\Phi = 0.1$ of slip spheres at $Re = 100$ and 200 is numerically studied. For small values of slip number, the flow is attached to the slip spheres whereas for large values of the slip number, a small recirculation wake has been observed. The angle of separation and wake length decreases with decreasing slip number. The surface pressure and surface vorticity distributions are found to be significantly affected by the slip boundary condition. The individual and total drag coefficients are found to decrease with the decreasing slip number and/or with the increasing Reynolds number. However, the ratio between the pressure and friction drag coefficients increases with the increasing Reynolds number.

References

1. Hatzikiriakos, S.G.: Wall slip of molten polymers. *Prog. Polym. Sci.* **37**, 624–643 (2012)
2. Moshfegh, M., Shams, G., Ebrahim, A.R.: A novel slip correction factor for spherical aerosol particles. *Eng. Technol.* **46**, 108–114 (2008)
3. Elasm, L., Feuillebois, F.: Green function for a Stokes flow near a porous slab. *ZAMP* **81**, 743–752 (2001)
4. Chilcott, M.D., Rallison, J.M.: Creeping flow of dilute polymer solutions past cylinders and spheres. *J. Nonnewton. Fluid Mech.* **29**, 381–432 (1988)
5. Sochi, T.: Slip at fluid-solid interface. *Polym. Rev.* **51**, 309–340 (2011)
6. Palani, N., Ramalingam, V., Ramadoss, G., Seeniraj, R.V.: Study of slip velocity and application of drift-flux model to slip velocity in a liquid-solid circulating fluidized bed. *Adv. Powder Technol.* **22**, 77–85 (2011)

7. Hatzikiriakos, S.G., Dealy, J.M.: Wall slip of molten high density polyethylene: II. Capillary rheometer studies. *J. Rheol.* **36**, 703–741 (1992)
8. Hatzikiriakos, S.G., Dealy, J.M.: Wall slip of molten high density polyethylene: I. Sliding plate rheometer studies. *J. Rheol.* **35**, 497–523 (1991)
9. Luk, S., Mutharasan, R., Apelian, D.: Experimental observation of wall slip: tube and packed bed flow. *Ind. Eng. Chem. Res.* **26**, 1609–1616 (1987)
10. Denn, M.M.: Extrusion instabilities and wall slip. *Ann. Rev. Fluid Mech.* **22**, 265–287 (2001)
11. Neto, C., Evans, D.R., Bonaccorso, E., Butt, H.J., Craig, V.S.J.: Boundary slip in Newtonian liquid: a review of experimental studies. *Rep. Prog. Phys.* **68**, 2859–2897 (2005)
12. Keh, H.J., Chen, S.H.: The motion of a slip spherical particle in an arbitrary Stokes flow. *Eur. J. Mech. B/Fluids* **15**, 791–807 (1996)
13. Datta, S., Singhal, S.: Slip flow past a sphere with a source at its centre. *Int. J. Appl. Math. Mech.* **7**, 36–51 (2011)
14. Kumar, A., Hodgson, P., Fabijanic, D., Gao, W.: Numerical solution of gas-solid flow in fluidized bed at sub-atmospheric pressures. *Adv. Powder Technol.* **23**, 485–492 (2012)
15. Luo, H., Pozrikidis, C.: Effect of surface slip on Stokes flow past a spherical particle in infinite fluid and near a plane wall. *J. Eng. Math.* **62**, 1–21 (2008)
16. Reed, L.D., Morrison, F.A.: Particle interactions in viscous flow at small values of Knudsen number. *J. Aerosol Sci.* **5**, 175–189 (1974)
17. Padmavathi, B.S., Amaranath, T., Nigam, S.D.: Stokes flow past a sphere with mixed slip-stick boundary conditions. *Fluid Dyn. Res.* **11**, 229–234 (1993)
18. Faltas, M.S., Saad, E.I.: Stokes flow past an assemblage of slip eccentric spherical particle-in-cell models. *Math. Methods Appl. Sci.* **34**, 1594–1605 (2011)
19. Happel, J.: Viscous flow in multiparticle systems: slow motion of fluids relative to beds of spherical particles. *AIChE J.* **4**, 197–201 (1958)
20. Kuwabara, S.: The forces experienced by randomly distributed parallel cylinders or spheres in a viscous flow at small Reynolds numbers. *J. Phys. Soc. Jpn.* **14**, 527–532 (1959)
21. Bird, B.R., Stewart, W.E., Lightfoot, E.N.: *Transport Phenomena*. John-Wiley, New York (1987)
22. Harlow, F.H., Welch, J.E.: Numerical calculation of time-dependent viscous incompressible flow of fluid with free surfaces. *Phys. Fluids* **8**, 2182–2188 (1965)
23. Leonard, B.P.: A stable and accurate convective modeling procedure based on quadratic upstream interpolation. *Comput. Methods Appl. Mech. Eng.* **19**, 59–98 (1979)
24. Gummalam, S., Chhabra, R.P.: Rising velocity of swarm of bubbles in a power-law non-Newtonian liquid. *Can. J. Chem. Eng.* **65**, 1004–1008 (1987)
25. Jaiswal, A.K., Sundararajan, T., Chhabra, R.P.: Flow of power law liquids through particle assemblages at intermediate Reynolds numbers. *Can. J. Chem. Eng.* **69**, 1235–1241 (1991)

Fluid Mechanics and Fluid Power – Contemporary
Research

Proceedings of the 5th International and 41st National
Conference on FMFP 2014

Saha, A.K.; Das, D.; Srivastava, R.; Panigrahi, P.K.;
Muralidhar, K. (Eds.)

2017, XXIV, 1701 p. 1095 illus. In 2 volumes, not
available separately., Softcover

ISBN: 978-81-322-2741-0